Hyperuniformity in amorphous silicon based on the measurement of the infinite-wavelength limit of the structure factor

Ruobing Xie[a,1], Gabrielle G. Long[a,b], Steven J. Weigand[c], Simon C. Moss[d,2], Tobi Carvalho[e], Sjoerd Roorda[e], Miroslav Hejna[f], Salvatore Torquato[f,g], and Paul J. Steinhardt[f,h,3]

[a]X-Ray Science Division, Argonne National Laboratory, Argonne, IL 60439; [b]Material Measurement Laboratory, National Institute of Standards and Technology, Gaithersburg, MD 20899; [c]DuPont-Northwestern-Dow Collaborative Access Team Synchrotron Research Center, Northwestern University, Argonne National Laboratory, Argonne, IL 60439; [d]Department of Physics and Texas Center for Superconductivity, University of Houston, Houston TX 77204; [e]Département de Physique, Université de Montréal, Montréal, QC, Canada H3C 3J7; and [f]Department of Physics, [g]Department of Chemistry and Princeton Institute for the Science and Technology of Materials, and [h]Princeton Center for Theoretical Science, Princeton University, Princeton, NJ 08544

Edited by T. C. Lubensky, University of Pennsylvania, Philadelphia, PA, and approved June 27, 2013 (received for review November 20, 2012)

We report the results of highly sensitive transmission X-ray scattering measurements performed at the Advanced Photon Source, Argonne National Laboratory, on nearly fully dense high-purity amorphous-silicon (a-Si) samples for the purpose of determining their degree of hyperuniformity. A perfectly hyperuniform structure has complete suppression of infinite-wavelength density fluctuations, or, equivalently, the structure factor $S(q\rightarrow 0) = 0$; the smaller the value of $S(0)$, the higher the degree of hyperuniformity. Annealing was observed to increase the degree of hyperuniformity in a-Si where we found $S(0) = 0.0075\ (\pm 0.0005)$, which is significantly below the computationally determined lower bound recently suggested by de Graff and Thorpe [de Graff AMR, Thorpe MF (2010) *Acta Crystallogr A* 66(Pt 1):22–31] based on studies of continuous random network models, but consistent with the recently proposed nearly hyperuniform network picture of a-Si. Increasing hyperuniformity is correlated with narrowing of the first diffraction peak and extension of the range of oscillations in the pair distribution function.

glass | disordered solid

After more than a half century of theoretical efforts and increasingly precise measurements, understanding the atomic-scale structure of disordered solids remains an outstanding challenge (1). Interest in this area continues unabated, as the link between structure and physical properties is key to the design of functional materials.

In this paper, we examine the behavior of the structure factor $S(q)$ in the infinite-wavelength ($q\rightarrow 0$) limit for high-purity amorphous silicon (a-Si) to determine its degree of hyperuniformity. The structure factor $S(q)$ is given by $S(q) = \frac{1}{N}\langle \sum_{jk} e^{-iq(R_j - R_k)} \rangle$, where $q = (\frac{4\pi}{\lambda})\sin\theta$, N is the number of atoms, R_j and R_k are their positions, λ is the X-ray wavelength, and 2θ is the scattering angle. By definition, a perfectly hyperuniform structure has infinite-wavelength density fluctuations that are completely suppressed and, hence, its structure factor $S(q\rightarrow 0) = 0$ (2). In general, the value $S(q\rightarrow 0)$ measures the degree of hyperuniformity.

Ordered solids such as crystalline and quasicrystalline materials are trivially perfectly hyperuniform. Although liquids are nonhyperuniform, it is possible to have isotropic disordered solid structures that are perfectly hyperuniform (2). This special class includes "maximally random jammed" (MRJ) packings of equal-sized spheres, for which it has been shown that $S(q\rightarrow 0)$ vanishes linearly with q (3). Moreover, one can explicitly construct a wide class of disordered hyperuniform point patterns using a "collective-coordinate" approach (4).

Determining where amorphous silicon falls in this spectrum was motivated by recent research on hyperuniform disordered photonic materials that exhibit complete (both polarizations and all directions) and sizable photonic band gaps (5). Florescu et al. (5) have argued that the existence of photonic bandgaps in disordered photonic solids may be explained using theoretical ideas similar to those introduced by Weaire and Thorpe to explain the electronic bandgap in amorphous semiconductors (6). Although strict hyperuniformity is not required to have an electronic bandgap according to the Weaire–Thorpe argument, the Florescu et al. study of photonic bandgaps in hyperuniform versus nonhyperuniform photonic solids led them to conjecture that the electronic bandgap in amorphous silicon should increase with the degree of hyperuniformity; that is, samples with smaller $S(q\rightarrow 0)$ should have improved bandgap properties. This naturally led us to ask the question: How close to zero can $S(q\rightarrow 0)$ get in amorphous silicon?

Theoretically, it is possible to construct network models of a-Si with increasing degrees of hyperuniformity (7). Beyond satisfying certain topological properties, an appropriate model must obey geometrical constraints on the distribution of bond distances and bond angles to be in accord with observations. Recent work by de Graff and Thorpe (8) suggests that geometric constraints may be incompatible with hyperuniformity. More specifically, they suggest a lower bound of $S(q\rightarrow 0) = 0.035 \pm 0.001$, based on their computer simulations of a 100,000-atom continuous random network (CRN) model for amorphous silicon, the largest such network model to date, relaxed using a Keating potential. Moreover, they point out that their bound is consistent with approximating amorphous silicon as a frozen liquid, whose density fluctuations have a similar value. However, we have recently shown by explicit constructions (7) that it is theoretically possible to produce a spectrum of network structures with the same topology and nearly identical bond distance and angle distributions as CRN models but with lower values of $S(q\rightarrow 0)$. These constructions include what we term "nearly hyperuniform network models," i.e., those structures possessing $S(q\rightarrow 0)$ values that are at least 50% smaller than that of the aforementioned CRN model. Thus, it is not really clear how small $S(q\rightarrow 0)$ can be in amorphous silicon (7).

These theoretical considerations have motivated us to measure the degree of hyperuniformity in some of the best-characterized experimental samples (9, 10) of nearly fully dense amorphous silicon. Pure, fully dense a-Si is difficult to prepare as it is

Author contributions: R.X., G.G.L., S.J.W., S.C.M., and P.J.S. designed research; R.X., G.G.L., S.J.W., and S.C.M. performed research; T.C. and S.R. contributed new reagents/analytic tools; R.X., G.G.L., S.R., M.H., S.T., and P.J.S. analyzed data; and R.X., G.G.L., S.R., S.T., and P.J.S. wrote the paper.

The authors declare no conflict of interest.

This article is a PNAS Direct Submission.

[1]Present address: Shanghai Synchrotron Radiation Facility, Shanghai 201204, China.

[2]Deceased March 14, 2011.

[3]To whom correspondence should be addressed. E-mail: steinh@princeton.edu.

overconstrained, and hence is a highly strained material. More than a decade ago, Roorda et al. (11) perfected a method for preparing high-purity examples of a-Si by means of self-ion implantation into a Si (001) wafer and subsequent removal of the remaining single-crystal substrate. The edge-supported, fully dense, bulk (12-μm-thick) a-Si samples from the earlier Laaziri work (9, 10) were used in this investigation into possible hyperuniformity in a real and noncrystalline material.

We performed highly sensitive transmission X-ray scattering measurements at the Advanced Photon Source (APS) to follow the course of $S(q)$ in the limit as $q \to 0$. As we demonstrate below, we find that the scattering from an annealed (relaxed) a-Si sample is nearly hyperuniform. An analysis of the X-ray scattering features further reveals that improved hyperuniform ordering is associated with increasingly uniform short-range tetrahedral ordering.

Samples and Scattering Measurements

The samples are nearly fully dense a-Si prepared (11) by means of self-ion implantation at 12 different energies and fluences at 77 K into single-crystal Si (001). One of the 12-μm-thick a-Si membranes on single-crystal Si substrates was annealed in vacuum at 600 °C for 1 h to create an annealed "relaxed" structure, whereas another was "as-implanted." A wet chemical etch was applied to a 5-mm–diameter area in the center of the back of each 2 cm × 2 cm wafer, removing the crystalline silicon (c-Si) and leaving a freestanding, edge-supported membrane of high-purity a-Si.

We used a (250 μm × 250 μm) beam of 17-keV X-rays, in vacuum, and a sample-to-detector distance of 293 mm to measure the scattering intensity in the transmission geometry from each of the membranes. The measurements were immediately repeated with 9-keV X-rays to cover a combined scattering vector range from $q = 0.08$ Å^{-1} to 2.4 Å^{-1}. The 17-keV data included the first diffraction peak near $q = 2$ Å^{-1}. This was important for two reasons. It enabled us to verify that the amorphous scattering volume was free from nucleation of nanocrystalline silicon. If nucleation were present, it would be detected through the appearance of a very sharp tiny (111) scattering feature on the principle peak. Second, as the extended $S(q)$ oscillates about unity, it made possible a comparison with the full scattering curve that had been measured earlier out to $q = 55$ Å^{-1} (9, 10). These samples, which had been investigated extensively in 1998, are remarkably stable, yielding the same measured results for $S(q)$ from the annealed (relaxed) and the as-implanted samples as those from more than a decade earlier.

The X-ray scattering intensity data were corrected for detector dark field, intensity calibration, sample absorption, and X-ray polarization factor. Our first calibration was made by means of a rotating glassy carbon secondary standard previously measured on the absolute-calibrated APS Ultra-Small Angle X-ray Scattering (USAXS) instrument (12). The new scattering intensity data corresponded exactly to the earlier data (9, 10) after we set the sample thicknesses to 12.7 μm as determined from an independent absolute calibrated USAXS measurement. This internal consistency assures the integrity of the measurements.

The calibrated intensity was converted to $S(q)$ in electron units/atom making use of published atomic scattering factors (13) and the known density of our a-Si. Fig. 1 shows the experimentally determined $S(q)$ for the two samples. The intensity of the first diffraction peak is greater and the peak width is narrower for the annealed (relaxed) a-Si than for the as-implanted a-Si. The curves cross at $q \sim 1.75$ Å^{-1}, below which more scattering is recorded in the scattering curve from the as-implanted sample.

To examine whether there was any structural memory in the a-Si of the c-Si from which it was created, we did an X-ray cross-correlation analysis (14) of scattering intensity around the principal peak diffraction ring and found no anisotropy or preferred

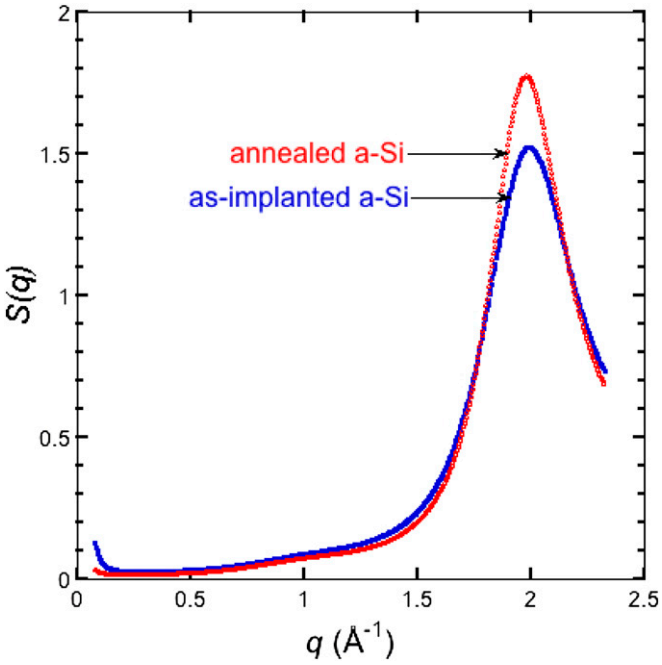

Fig. 1. Experimental $S(q)$ for the as-implanted a-Si (solid squares) and the annealed (relaxed) a-Si (open triangles).

directions within either of the edge supported a-Si membranes. Analysis of the intensity distribution around the ring yielded the same result. Similar analyses of a-Si on c-Si showed well-defined anisotropy at the amorphous-Si-to-crystalline-Si interface along the Si <110> directions (15).

Results and Discussion

At the lowest values of q, there is an upturn in the measured $S(q)$ that we attribute mainly to small-angle scattering from surface roughness and secondarily from a very small amount of nanoporosity. Scattering from surface roughness is expected because one side of the samples is matte rather than shiny as a result of the chemical etch that was used to remove the crystal substrate. A new sample was made by direct ion implantation into a 10-μm-thick c-Si membrane that had been polished on both sides. Indeed, in this sample the upturn in the measured $S(q)$ was much reduced. Because large q-range (2.5–55 Å^{-1}) data were not available for this sample, we continued the analysis of the older (etched) samples.

Before correcting for the small-angle scattering, we can derive an upper limit on $S(q \to 0)$ by extrapolating a flat line from the minimum value of $S(q)$ to $q = 0$. This procedure yields $S(0)_{\text{upper limit}} = 0.026$ and 0.016 for the as-implanted and annealed (relaxed) a-Si, respectively. Note that these values are below the computationally determined lower bound of $S(0) = 0.035$ suggested by de Graff and Thorpe (8), and that the value for annealed a-Si is lower than that for as-implanted a-Si.

Of greater interest than the singular value of $S(0)$ is how the measured $S(q)$ behaves as $q \to 0$. To determine this, we fit $S(q)$ between $q = 0.08$ and 0.4 Å^{-1} to the form $S(q) = a\,q^b + S(q \to 0) + S'(q \to 0)\,q$, where the first term is an approximation to the small-angle X-ray scattering (i.e., including both Guinier and Porod scattering from a range of surface feature sizes) and the last terms describe the linear contribution to $S(q)$ at small q. The measured $S(q)$, the best overall fits, and the best-fit linear contribution are shown in Fig. 2, where the fit is shown with solid lines. The exponent b, representing the surface scattering, is -3.34 ± 0.02 for the as-implanted sample and -2.40 ± 0.03 for the

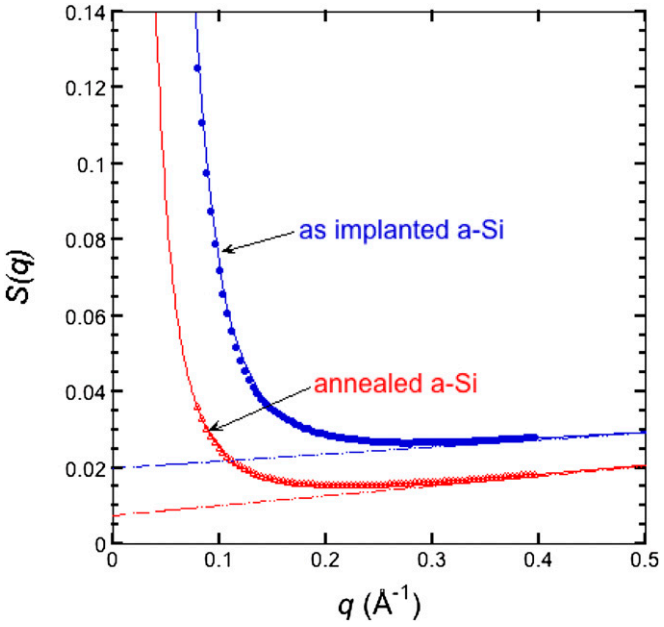

Fig. 2. *S(q)* at low *q* for the as-implanted a-Si (solid circles) and the annealed (relaxed) a-Si (open triangles). Note that the minimum *S(q)* for both as-implanted and annealed is less than 0.03, below the theoretical bound based on CRN models relaxed with Keating potentials or on treating a-Si as a frozen liquid (7). To obtain $S(q\to0)$, the data are fit (solid curves) to a sum of an inverse power law in *q*, representing small angle scattering mostly from a rough etched surface, and a linear contribution. The dashed lines show the linear contribution only. The plot shows that this ansatz fits well (see text for details). We measure the degree of hyperuniformity to be $S(q\to0) = 0.0199 \pm 0.0005$ for the as-implanted and $S(q\to0) = 0.0075 \pm 0.0005$ for the annealed a-Si.

annealed (relaxed) sample. The linear portion of the fit is shown with dashed lines. We find that $S(q\to0) = 0.0199 \pm 0.0005$ and 0.0075 ± 0.0005 for the as-implanted and annealed (relaxed) a-Si, respectively. It is clear that annealing increases the degree of hyperuniformity, although both are consistent with nearly hyperuniform network models (7) and both have $S(q\to0)$ significantly lower than the de Graff–Thorpe lower bound (8).

We have also considered the more general six-parameter fitting function of the form $S(q) = a\,q^b + c\,q^d + S(q\to0) + S'(q\to0)\,q$. We find that the best-fit $S(q\to0)$ is less than the value reported above with essentially the same goodness of fit. Hence, the values above could be considered conservative upper bounds.

The values of the terminal slopes are 0.0188 (± 0.0009) Å and 0.0260 (± 0.0005) Å for the as-implanted and annealed (relaxed) a-Si, respectively. It is noteworthy that the linear approximation is a good fit to the behavior of *S(q)* for small wavenumber and agrees with what has been observed in MRJ sphere packings (4).

When we combine results from earlier studies (9, 10) with those from the present work, we note that the radial distribution function (RDF) indicated that a number of changes were induced by thermal annealing: increased coordination number C_1, narrower tetrahedral angle distribution $\Delta\Theta$, and increased dihedral angle ordering $F(\varphi)$. Recent analysis (16) also found extended range density oscillations in the pair distribution function with an exponential decay length Λ that increased upon annealing, and with a periodicity close to the size of a tetrahedral Si unit. Each of these parameters [C_1, $\Delta\Theta$, $F(\varphi)$, or Λ] can be taken as an indicator of the state of relaxation of the network.

The experiment in refs. 9 and 10 found that the nearest-neighbor coordination number C_1 goes from 3.79 to 3.88 when a-Si is thermally annealed. This result implies that annealed a-Si is closer to ideal nearly hyperuniform network models (7) than as-implanted a-Si, as will be discussed further below.

The bond angle distribution $\Delta\Theta$ for our as-implanted and annealed samples was reported as 10.45° ± 0.09° and 9.63° ± 0.08°, respectively (10). These experimental values were derived from the width of the second peak in the radial distribution function. It has since been found (16) that the second peak includes a contribution from third-nearest neighbors and that the value for $\Delta\Theta$, as deduced from the width of the second peak, may be overestimated by 1.5°.

Thermal annealing of our samples also led to the appearance of a small feature in the RDF around 4.8 Å, indicating ordering of the dihedral angles. The decay length Λ of the extended range density oscillations observed in our samples (16) increased upon annealing from 1.2 ± 0.4 to 1.8 ± 0.3 bond lengths. Indeed, the physical properties of a-Si will vary according to the preparation method (e.g., pressure induced instead of ion implantation), but thermal annealing leads to a convergence of those properties to a relatively well-defined common state (17).

The 10^5-atom model (8) used to predict $S(q\to0)$ of a-Si made use of the Keating interatomic potential; several other properties that the model calculates demonstrate why it may overestimate the limit of long-wavelength scattering. For example, the width of the bond angle distribution (at 9.6°), the lack of third neighbor ordering (18), and the long-range ordering decay length (at 0.89 bond lengths) all indicate that the model is perhaps best viewed as one describing a form of a-Si even less structurally relaxed than our as-implanted material. By contrast, a spectrum of nearly hyperuniform network models (7) has been constructed with $S(q\to0)$ ranging from 0.035 to values comparable to the experimental values reported here, while maintaining virtually the same bond distance and bond angle distribution as CRN models.

Nearly hyperuniform network models (7) are derived by means of a two-step numerical protocol that combines the Keating and Stillinger–Weber potentials. The first step is a standard bond-switching annealing procedure using a Keating potential (19) that is augmented with Barkema–Mousseau modifications (20). However, unlike the Barkema–Mousseau CRN model, the structures are annealed between 2 and 250 times longer to achieve a sequence of inherent structures (local potential-energy minima) that have lower energies than those of the Barkema–Mousseau CRN model. In the second step, each of the configurations obtained via a Keating potential is used as the initial condition for atomic-position rearrangement under a modified Stillinger–Weber potential (21) at zero pressure via a conjugate gradient method. With this two-step procedure, the resulting structures possess a negligible number of dangling bonds. In Fig. 3, we show $S(0)$ as a function of the inverse of the height of the first scattering peak in *S(q)* for the Barkema–Mousseau CRN model (8), for the Keating anneals, and for the subsequent Stillinger–Weber quenches. The experimental values of $S(0)$ for the as-implanted and annealed a-Si samples, also shown in Fig. 3, are consistent with the nearly hyperuniform network picture.

Recent fluctuation electron microscopy (FEM) measurements combined with electron diffraction have led to the suggestion (22, 23) that as-prepared a-Si possesses topology closely related to crystalline silicon, or that it is "paracrystalline." In particular, the claim is that a-Si is heterogeneous on a nanometer-length scale and consists of paracrystallites embedded in a disordered (not necessarily CRN) matrix (23). If this were correct, it could be argued that $S(q\to0)$ would be expected to vanish or be very small. The paracrystalline argument, however, is inconsistent with the trends observed in our data. FEM has repeatedly inferred that annealing of a-Si leads to a reduction in the paracrystallinity by a factor of 2–10 (17, 24–26), thus predicting that $S(q\to0)$ should be lower in the as-implanted material than in the annealed material. This is the opposite of what we observe. We conclude that our observed low value for $S(q\to0)$ is indeed

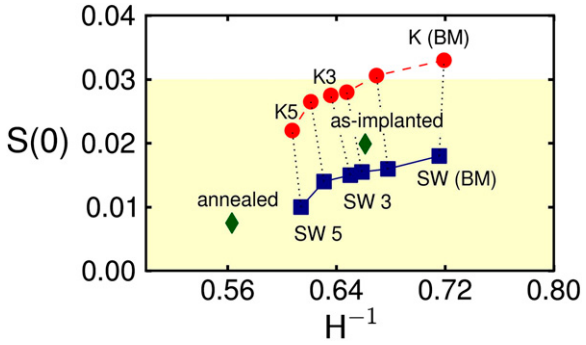

Fig. 3. Values of $S(0)$ for the network structural models progressively relaxed with a Keating potential as a function of the inverse height H of the first scattering peak. Solid red circles [with examples labeled by K(BM)] represent the original Barkema–Mousseau model and $K1$ through $K5$ is a series of progressive relaxations. The Keating-relaxed models serve as initial conditions for the subsequently quenched Stillinger–Weber structures, which appear as solid blue squares (with corresponding examples labeled by SW). Experimental values for as-implanted a-Si and annealed a-Si appear as solid green diamonds. The trajectory of the experimental values fits well with the modified Stillinger–Weber results. The shaded region below $S(0)$ = 0.03 indicates the nearly hyperuniform range in which $S(0)$ is below the equilibrium melting value for a-Si.

a signature of hyperuniformity consistent with the nearly hyperuniform network picture (7).

$S(q)$ for both as-implanted and annealed samples exhibits a small broad peak that was observed previously (9, 10). This feature is close to $q = 1$ Å^{-1} and well below the first diffraction peak near $q = 2$ Å^{-1} (Fig. 1). Diffraction peaks between $q = 1$ and 2 Å^{-1} have been a subject of intense interest (27, 28) because their appearance at low q indicates that they arise from intermediate range ordering at distances of order > 4 Å rather than from nearest neighbors. It thus offers potential insights into the packing of structural clusters. For glasses that include two or more atomic species, a prepeak has been explained in terms of chemical clustering and concentration–concentration correlations. In metallic glasses, the prepeak has been associated with minority species ordering (29). However, for a disordered material consisting of a single element such as a-Si, such interpretations are not possible. A possible explanation is the presence of a small number of vacancies or vacancy clusters (29–31); these vacancies would need to be partially ordered for the prepeak to appear. If indeed the intensity of the small feature scales with vacancy–vacancy correlations, then this would be consistent with the fact that there are fewer vacancies in our annealed (relaxed) a-Si with coordination ~3.88 than in the as-implanted a-Si with coordination of ~3.79. We note, however, that the small feature has been found in nearly hyperuniform network models without dangling bonds or defects (7).

The high degree of hyperuniformity, and the observation that thermal annealing not only relaxes the a-Si but also increases the degree of hyperuniformity, provides insights into the nature of a-Si. Other properties of a-Si, such as the Raman transverse-optical–like peak width (32, 33), metal impurity solubility and diffusivity (34), and carrier lifetime and electronic density of states (35), have been observed to undergo changes upon thermal annealing, all showing that annealed a-Si is a better-defined, less-defected, lower-energy state than as-prepared a-Si (36). One such property that concerns us in particular is the bandgap, in view of the prediction that a higher degree of hyperuniformity is related to a larger bandgap. Preliminary calculations (7) show that the bandgap increases as the degree of hyperuniformity increases.

Bandgaps for pure a-Si (not hydrogenated a-Si:H), derived from measured complex dielectric functions, vary depending on the preparation history (37), where self-ion-implanted samples had a bandgap of 0.85 eV, evaporated samples had a bandgap of 1.12 eV, but annealed samples (3 h at 500 °C) had the broadest bandgap of 1.30 eV (35, 38). Indeed, the largest measured bandgap of a-Si was observed in annealed material, which exhibits the largest degree of hyperuniformity, confirming the predicted behavior.

Summary

High-sensitivity X-ray scattering data indicate that as-implanted and annealed (relaxed) a-Si have a nearly hyperuniform disordered atomic structure. The observed value of $S(q\to0) = 0.0075$ (±0.0005) for annealed a-Si is significantly smaller than the theoretical lower bound offered by de Graff and Thorpe. Furthermore, annealing increases the degree of hyperuniformity [$S(q\to0)$ is smaller]. Because both as-implanted and annealed a-Si have smaller $S(q\to0)$ than found for the largest current continuous random network models based on the Keating potential, it is fair to conclude that these models and approximations fail to explain the structure of nearly fully dense amorphous silicon. On the other hand, the result is consistent with nearly hyperuniform network model studies (7) that have led to large computer models that produce $S(q\to0)$ well below the lower bound on $S(q\to0)$ values suggested by de Graff–Thorpe (8) while maintaining reasonable bond distance and bond angle distributions.

Our present study demonstrates that $S(q\to0)$ is a useful figure-of-merit for comparing amorphous network solids, such as amorphous silicon. Although we do not have enough samples in our study to investigate the issue here, further information is contained in the shape of $S(q)$ as $q\to0$: in the case of our samples, the linear behavior in our samples and the associated slope. We note that hyperuniform MRJ packings consisting of nonspherical particles have a spectral function that goes to zero linearly for small q, and the associated slope is related to the degree of shape anisotropy (39). Investigations of $S(q\to0)$ and the shape as $q\to0$ for photonic solids suggest that they correlate with photonic bandgap properties. Here, we observe that the same holds for the electronic bandgap and perhaps other physical properties (e.g., mechanical properties) in amorphous semiconductors.

ACKNOWLEDGMENTS. We thank Mike Thorpe for discussions during the early portion of this research and Jan Ilavsky for help with the ultra small-angle X-ray scattering (USAXS) measurements. This research was performed mainly at the SAXS/wide-angle X-ray scattering (WAXS) instrument at DuPont-Northwestern-Dow Collaborative Access Team 5-ID-D and also at the USAXS instrument at 32-ID-B at the Advanced Photon Source, Argonne National Laboratory. Use of the APS is supported by the US Department of Energy, Office of Science, under Contract DE-AC02-006CH11357. This work is supported in part by the National Science Foundation-Materials Research Science and Engineering Center Program through New York University (DMR-0820341 to S.T. and P.J.S.) and by the Natural Sciences and Engineering Research Counsel of Canada and Fonds de Recherche Nature et Technologies Québec (S.R. and T.C.).

1. Salmon PS (2006) Decay of the pair correlations and small-angle scattering for binary liquids and glasses. *J Phys Condens Matter* 18:11443–11469.
2. Torquato S, Stillinger FH (2003) Local density fluctuations, hyperuniformity, and order metrics. *Phys Rev E* 68(4):041113.
3. Donev A, Stillinger FH, Torquato S (2005) Unexpected density fluctuations in disordered jammed hard-sphere packings. *Phys Rev Lett* 95(9):090604.
4. Batten RD, Stillinger FH, Torquato S (2008) Classical disordered ground states: Super-ideal gases, and stealth and equiluminous materials. *J Appl Phys* 104(3):033504.
5. Florescu M, Torquato S, Steinhardt PJ (2009) Designer disordered materials with large, complete photonic band gaps. *Proc Natl Acad Sci USA* 106(49):20658–20663.
6. Weaire D, Thorpe MF (1971) Electronic properties of an amorphous solid. I. A simple tight binding theory. *Phys Rev B* 4(8):2508–2520.
7. Hejna M, Steinhardt PJ, Torquato S (2013) Nearly hyperuniform network models of amorphous silicon. *Phys Rev B* 87(24):245204.
8. de Graff AMR, Thorpe MF (2010) The long-wavelength limit of the structure factor of amorphous silicon and vitreous silica. *Acta Crystallogr A* 66(Pt 1):22–31.

9. Laaziri K, et al. (1999) High resolution radial distribution function of pure amorphous silicon. *Phys Rev Lett* 82(17):3460–3463.
10. Laaziri K, et al. (1999) High-energy X-ray diffraction study of pure amorphous silicon. *Phys Rev B* 60(19):13520–13533.
11. Roorda S, Laaziri K, Gujrathi SC (1999) Edge supported amorphous silicon membranes for diffraction studies. *Nucl Instrum Methods Phys Res B* 148:360–365.
12. Ilavsky J, et al. (2009) Ultra-small angle scattering at the Advanced Photon Source. *J Appl Cryst* 42:469–479.
13. Waasmaier D, Kirfel A (1995) New analytical scattering factor functions for free atoms and ions. *Acta Crystallogr A* 51:416–431.
14. Wochner P, et al. (2009) X-ray cross correlation analysis uncovers hidden local symmetries in disordered matter. *Proc Natl Acad Sci USA* 106(28):11511–11514.
15. Xie R, Long GG, Moss SC, Roorda S (2011) Order and disorder in freestanding pure amorphous silicon and amorphous silicon over Si(001). *J Non-Cryst Solids* 357:2498–2501.
16. Roorda S, et al. (2012) Disentangling neighbors and extended range density oscillations in monatomic amorphous semiconductors. *Phys Rev Lett* 108(25):255501.
17. Haberl B, et al. (2009) Structural characterization of pressure-induced amorphous silicon. *Phys Rev B* 79(15):155209.
18. Nakhmanson SM, Voyles PM, Mousseau N, Barkema GT, Drabold DA (2001) Realistic models of paracrystalline silicon. *Phys Rev B* 63(23):235207.
19. Djordjevic BR, Thorpe MF, Wooten F (1995) Computer model of tetrahedral amorphous diamond. *Phys Rev B Condens Matter* 52(8):5685–5689.
20. Barkema GT, Mousseau N (2000) High quality continuous random networks. *Phys Rev B* 62(8):4985–4990.
21. Vink RLC, Barkema GT, van der Weg WF, Mousseau N (2001) Fitting the Stillinger-Weber potential to amorphous silicon. *J Non-Cryst Solids* 282:248–255.
22. Gibson JM, Treacy MMJ, Sun T, Zaluzec NJ (2010) Substantial crystalline topology in amorphous silicon. *Phys Rev Lett* 105(12):125504.
23. Treacy MMJ, Borisenko KB (2012) The local structure of amorphous silicon. *Science* 335:950–953.
24. Haberl B (2010) Structural characterization of amorphous silicon. PhD thesis (Australian Natl Univ, Canberra, Australia).
25. Haberl B, et al. (2011) Unexpected short- and medium-range atomic structure of sputtered amorphous silicon upon thermal annealing. *J Appl Phys* 110(9):096104.
26. Cheng J-Y, Gibson JM, Jacobson DC (2001) Observations of structural order in ion-implanted amorphous silicon. *J Mater Res* 16(11):3030–3033.
27. Moss SC, Price DL (1985) *Random Packing of Structural Units and the First Sharp Diffraction Peak in Glasses. Physics of Disordered Materials*, eds Adler D, Fritzsche H, Ovshinsky SR (Plenum, New York), pp 77–94.
28. Price DL, Moss SC, Reijers R, Saboungi M-L, Susman S (1989) Intermediate-range order in glasses and liquids. *J Phys Condens Matter* 1(5):1005–1008.
29. Steeb S, Lamparter P (1984) Diffraction studies of liquid and amorphous-alloys. *J Non-Cryst Solids* 61-62:237–248.
30. Elliott SR (1991) Origin of the first sharp diffraction peak in the structure factor of covalent glasses. *Phys Rev Lett* 67(6):711–714.
31. Blétry J (1990) Sphere and distance models for binary disordered systems. *Philos Mag B* 62(5):469–508.
32. Tsu R, Gonzalez-Hernandez J, Pollak FH (1984) Determination of energy barrier for structural relaxation in a-Si and a-Ge by Raman-scattering. *J Non-Cryst Solids* 66: 109–114.
33. Tsu R, Gonzalez-Hernandez J, Pollak FH (1985) Determination of the energy barrier for structural relaxation in amorphous Si and Ge by Raman-scattering. *Solid State Commun* 54(5):447–450.
34. Coffa S, Poate JM, Jacobson DC, Frank W, Gustin W (1992) Mechanisms of ion-beam-enhanced diffusion in amorphous-silicon. *Phys Rev B* 45(15):8355–8358.
35. Stolk PA, et al. (1994) Contribution of defects to electronic, structural, and thermodynamic properties of amorphous-silicon. *J Appl Phys* 75(11):7266–7286.
36. Roorda S, Doorn S, Sinke WC, Scholte PM, van Loenen E (1989) Calorimetric evidence for structural relaxation in amorphous silicon. *Phys Rev Lett* 62(16):1880–1883.
37. Fried M, Lohner T, Aarnink WAM, Hanekamp LJ, van Silfhout A (1992) Determination of complex dielectric functions of ion implanted and implanted-annealed amorphous silicon by spectroscopic ellipsometry. *J Appl Phys* 71(10):5260–5262.
38. Zammit U, et al. (1994) Optical-absorption studies of ion-implantation damage in Si on sapphire. *Phys Rev B Condens Matter* 49(20):14322–14330.
39. Zachary CE, Jiao Y, Torquato S (2011) Hyperuniformity, quasi-long-range correlations, and void-space constraints in maximally random jammed particle packings. II. Anisotropy in particle shape. *Phys Rev E* 83(5):051309.